

Physicochemical properties of pore residues predict activation gating of Ca_v1.2: A correlation mutation analysis

Stanislav Beyl · Katrin Depil · Annette Hohaus ·
Anna Sary-Weinzinger · Eugen Timin ·
Waheed Shabbir · Michaela Kudrnac · Steffen Hering

Received: 23 July 2010 / Revised: 14 September 2010 / Accepted: 15 September 2010 / Published online: 7 October 2010
© The Author(s) 2010. This article is published with open access at Springerlink.com

Abstract Single point mutations in pore-forming S6 segments of calcium channels may transform a high-voltage-activated into a low-voltage-activated channel, and resulting disturbances in calcium entry may cause channelopathies (Hemara-Wahanui et al., Proc Natl Acad Sci U S A 102 (21):7553–7558, 16). Here we ask the question how physicochemical properties of amino acid residues in gating-sensitive positions on S6 segments determine the threshold of channel activation of Ca_v1.2. Leucine in segment IS6 (L434) and a newly identified activation determinant in segment IIS6 (G1193) were mutated to a variety of amino acids. The induced leftward shifts of the activation curves and decelerated current activation and deactivation suggest a destabilization of the closed and a stabilisation of the open channel state by most mutations. A selection of 17 physicochemical parameters (descriptors) was calculated for these residues and examined for correlation with the shifts of the midpoints of the activation curve (ΔV_{act}). ΔV_{act} correlated with local side-chain flexibility in position L434 (IS6), with the polar accessible surface area of the side chain in position G1193 (IIS6) and with hydrophobicity in position I781 (IIS6). Combined descriptor analysis for positions I781 and G1193 revealed that additional amino acid properties may contribute to conformational changes during the gating process. The identified physicochemical

properties in the analysed gating-sensitive positions (accessible surface area, side-chain flexibility, and hydrophobicity) predict the shifts of the activation curves of Ca_v1.2.

Keywords Calcium channels · Pore stability · Activation determinants · Amino acid descriptors

Introduction

Calcium entry through voltage-gated calcium channels (Ca_v) initiates and controls a large variety of cellular functions such as generation and propagation of electrical impulses, sensory processes, muscle contraction, secretion of hormones and neurotransmitters, cell differentiation and gene expression [1]. Mammalian Ca²⁺ channel α_1 subunits are encoded by at least ten genes [7]. Depending on the potential where voltage-gated Ca²⁺ channels first open during a depolarisation (so-called threshold potential), they can be subdivided in high-voltage-activated (Ca_v1–Ca_v2) or low-voltage-activated (Ca_v3) Ca²⁺ channels. Different thresholds of activation were also reported for different isoforms of high-voltage-activated Ca²⁺ channels [7].

We have recently shown that a point mutation (I/T) in segment IIS6 of Ca_v1.2 that is associated with a channelopathy transforms the high-voltage-activated Ca_v1.2 channel into a low-voltage-activated channel [16, 19]. Additional gating-sensitive residues were identified in other S6 segments of Ca_v1.2 [22, 28].

The molecular mechanisms underlying channelopathy mutations in Ca_v1.2 are currently unknown. Ca_v1.2 are heterooligomeric protein complexes composed of an α_1 subunit and auxiliary β and α_2 - δ subunits (see [7] for review). Their pore-forming/voltage-sensing α_1 subunit is composed of four homologous domains formed by six transmembrane segments (S1–S6) each [6].

Stanislav Beyl and Katrin Depil contributed equally to this work.

Electronic supplementary material The online version of this article (doi:10.1007/s00424-010-0885-2) contains supplementary material, which is available to authorized users.

S. Beyl · K. Depil · A. Hohaus · A. Sary-Weinzinger · E. Timin ·
W. Shabbir · M. Kudrnac · S. Hering (✉)
Institute for Pharmacology and Toxicology, University of Vienna,
Althanstrasse 14,
1090 Vienna, Austria
e-mail: steffen.hering@univie.ac.at

Compared to Kv, the pore of Ca_v1.2 is asymmetric. The ‘helix-bending’ PXP motif of Kv1.2 is absent and the conserved glycine (corresponding to position 220 in KvAP and 83 in MthK, see [21]) is only present in segments IS6 and IIS6 (see review by Hering et al. [17]). We have shown that substituting proline for this glycine in IIS6 of Ca_v1.2 has minor effects on gating of Ca_v1.2 [19].

There is evidence, however, that Ca_v α₁ subunits share a common architecture with voltage-gated potassium channels. A cysteine scan of the pore-lining S6 segments of Ca_v2.1 by Zhen et al. [36] revealed that opening and closing of the channel changes the accessibility of cysteines in a pattern consistent with a gate localised on the intracellular side. This view is supported by pharmacological studies. On one hand, the inner channel mouth of Ca_v1.2 has to open to enable access of the charged (quaternary) phenylalkylamine devapamil (qDev) from the cytosolic side [3]. Interestingly, qDev has unrestricted (voltage independent) access to its binding pocket in the vestibule, suggesting a ‘widely open’ inner channel mouth in the open state that is in line with Poisson distribution of voltage in the open conformation of a potassium channel [21]. On the other hand, pore-forming S6 segments are apparently able to close the channel vestibule thereby restricting dissociation of organic Ca_v1.2 inhibitors such as qDev [3].

Scanning the pore-forming S6 segments with mutations to alanine [4], a bulky tryptophan, a ‘helix kinking’ proline, a small flexible glycine, a small polar threonine or aspartate or a small cysteine which can form disulphide bonds enabled the identification of gating-sensitive positions in the pore of various voltage-gated ion channels (e.g. [14, 19, 22, 27, 33, 35, 36]).

In the present study, we ask the question how physicochemical properties of amino acids in gating-sensitive positions of Ca_v1.2 S6 segments affect the threshold of channel activation (i.e. the open-closed equilibrium).

In continuation of our previous work, we focus on the ‘bundle-crossing region’ of segments IS6, IIS6 and IIIS6 where the channel is likely closed by tight sealing. G1193 was identified as a novel strong gating determinant in segment IIIS6. Systematic substitution of this residue with amino acids with different properties affected pore stability. A common kinetic phenotype was a leftward shift of the activation curve that is accompanied by decelerated channel deactivation (see also [3, 35]).

Pivotal physicochemical properties of mutated gating determinants in segments IS6, IIS6 and IIIS6 were identified by correlating magnitudes of the shifts of the activation curves with descriptors of the amino acids. By means of this ‘mutation correlation analysis’, we discovered significant links between activation gating and physicochemical properties in positions L434 (IS6), I781 (IIS6) and G1193 (IIIS6).

Materials and methods

Mutagenesis The Ca_v1.2 α₁-subunit coding sequence (GenBank™ X15539) in-frame 3′ to the coding region of a modified green fluorescent protein was kindly donated by Dr. M. Grabner et al. [12]. Substitutions in segment IS6 and IIIS6 of the Ca_v1.2 α₁-subunit were introduced using the QuikChange® Lightning Site-Directed Mutagenesis Kit (Stratagene) with mutagenic primers according to the manufacturer’s instructions. Mutations were introduced in segment IIIS6 in position 1193 (G1193T/V/N/M/A/Q/W/P) and positions F1191T, V1192T, F1194T, V1195T and I1196T and in IS6 in position 434 (L434A/G/T/V/N/S/W/M).

We systematically introduced residues of different sizes, polarity/hydrophobicity, and aromaticity. All constructs were checked by restriction site mapping and sequencing.

Cell culture and transient transfection Human embryonic kidney tsA-201 cells were grown at 5% CO₂ and 37°C to 80% confluence in Dulbecco’s modified Eagle’s/F-12 medium supplemented with 10% (v/v) foetal calf serum and 100 U/ml penicillin/streptomycin. Cells were split with trypsin/EDTA and plated on 35 mm Petri dishes (Falcon) at 30–50% confluence ~16 h before transfection. Subsequently, tsA-201 cells were co-transfected with cDNAs encoding wild-type or mutant Ca_v1.2 α₁-subunits with auxiliary β_{2a} [26] as well as α₂-δ₁ subunits [10]. The transfection of tsA-201 cells was performed using the FUGENE6 Transfection Reagent (Roche) following standard protocols. tsA-201 cells were used until passage number 15. No variation in channel gating related to different cell passage numbers was observed.

Ionic current recordings and data acquisition Barium currents (*I*_{Ba}) through voltage-gated Ca²⁺ channels were recorded at 22–25°C using the patch-clamp technique [15] by means of an Axopatch 200A patch-clamp amplifier (Axon Instruments, Foster City, CA, USA) 36–48 h after transfection. The extracellular bath solution contained (in millimolars) BaCl₂ 5, MgCl₂ 1, HEPES 10, and choline-Cl 140, titrated to pH 7.4 with methanesulphonic acid. Patch pipettes with resistances of 1 to 4 MΩ were made from borosilicate glass (Clark Electromedical Instruments, UK) and filled with pipette solution containing (in millimolars) CsCl 145, MgCl₂ 3, HEPES 10, and EGTA 10, titrated to pH 7.25 with CsOH. All data were digitised using a DIGIDATA 1200 interface (Axon Instruments, Foster City, CA, USA), smoothed by means of a four-pole Bessel filter and saved to disc. One hundred-millisecond current traces were sampled at 10 kHz and filtered at 5 kHz; tail currents were sampled at 50 kHz and filtered at 10 kHz. Holding potential of –100 mV was applied to exclude effects of

inactivation on measured parameters. Peak current at more positive holding potentials (−90 mV) was routinely measured to confirm complete recovery from inactivation. Leak currents were subtracted digitally using average values of scaled leakage currents elicited by a 10-mV hyperpolarizing pulse or electronically by means of an Axopatch 200 amplifier (Axon Instruments, Foster City, CA, USA). Capacity currents were not subtracted. When the pipettes were filled with pipette solution, their input resistance ranged between 1 and 4 MΩ. The mean cell capacity was 33 ± 5 pF ($n=12$). The mean series resistance was 4.7 ± 1.9 MΩ. It was compensated (60–85% compensation) by the following procedure: The depth of the positive feedback was gradually increased until oscillations (small overcompensation) appear. Even in large cells, the time constant of the capacity current (τ_{capacity}) did not exceed ≈ 0.25 ms. The early current phase was excluded from data processing (at least $3 \times \tau_{\text{capacity}} \approx 0.75$ ms). The pClamp software package (Version 7.0 Axon Instruments, Inc.) was used for data acquisition and preliminary analysis. Microcal Origin 7.0 was used for analysis and curve fitting.

Current–voltage (I–V) relationships for individual cells were normalized to the maximal current. Normalized I–V curves were averaged and the mean I–V curve was fitted to the modified Boltzmann equation:

$$I = \frac{G_{\text{max}} \cdot (V - V_{\text{rev}})}{1 + \exp\left(\frac{V_{0.5} - V}{k_{\text{act}}}\right)}$$

where I is the peak current, V is the membrane potential, V_{rev} is the reversal potential, G_{max} is the maximal membrane conductance, $V_{0.5}$ is the voltage for half-maximal activation and k_{act} is the slope factor.

The values of $V_{0.5}$ and k_{act} were used for calculation of the steady-state activation:

$$m_{\infty} = \frac{1}{1 + \exp\left(\frac{V_{0.5} - V}{k_{\text{act}}}\right)}$$

Data points for activation were calculated dividing the averaged peak currents at given potential by $G_{\text{max}} \times (V - V_{\text{rev}})$.

The time course of current activation was fitted to a mono-exponential function: $I(t) = A \times \exp\left(\frac{t}{\tau}\right) + C$, where $I(t)$ is the current at time t , A is the amplitude coefficient, τ is the time constant and C is the steady-state current. Data are given as mean \pm SE.

Calculation of amino acid descriptors Physicochemical descriptors were calculated for amino acids substituted in positions L434 (IS6), I781 (IIS6) and G1193 (IIIS6) using the Molecular Operating Environment (MOE; version 2008.10, Chemical Computing Group, Inc., Montreal, QC, Canada). This software package calculates more than 300 descriptors. Examples include polarity measures, size and

shape indices, flexibility, accessible surface area and others. Seventeen out of 327 possible descriptors were selected to analyse their potential role in channel gating (see Supplementary Tables 1 and 2 for list of descriptors and calculated values).

A turn propensity scale describing the relative turn preferences of the different amino acids in formation of transmembrane helical hairpins was taken from Monné et al. [25] (see also [34]). The hydrophobicity scales were taken from Kyte and Doolittle [23], Hessa et al. [18], White and Wimley [32], Guy [13], Eisenberg et al. [9] and Hopp and Woods [20]. Rigidity and flexibility indices accounting for a series of descriptors, i.e. number of bonds, number of rings, number of rings per atoms in molecule, number of rotatable bonds, number of rotatable bonds per atoms in molecule, number of rigid bonds (i.e. aromatic or double bonds), number of rigid bonds per atoms in molecule, longest flexible chain, ditto per atoms in molecule, number of rigid fragments, ditto per atoms in molecule, number of partial flexible chains and ditto per atoms in molecule, were taken from Gottfries and Eriksson [11].

Correlating amino acid properties with ΔV_{act} The capability of a given descriptor to predict the shift of the activation curve was established by ranking the correlation coefficients and its significance (t test). This approach enabled the identification of a ‘leading descriptor’, i.e. the one with the largest correlation coefficient (r) and the highest significance. Linear regressions were calculated using the ORIGIN subroutine which also yielded correlation coefficients and their statistical significance.

Subsequently, we correlated weighted linear combinations of all 17 descriptors with ΔV_{act} . Combined descriptors were calculated as $\Delta D = a\Delta D_1 + b\Delta D_2$ where ΔD s represent the difference between descriptor values for mutant and wild-type Ca_v1.2. Weighting factors (a and b) were used to estimate the contribution of each descriptor to correlation (see Table 3). For mutations in positions I781 (IIS6) and G1193 (IIIS6), this approach enabled us to establish a second descriptor of relevance by ranking the combined correlations with respect to the lowest root mean square error and the highest r (see Table 2).

Correlating amino acid properties with ΔG ΔG in the mutant channels relative to WT channel was calculated according to the equation:

$$\Delta G = RT \left(\frac{V_{0.5, \text{mut}}}{k_{\text{mut}}} - \frac{V_{0.5, \text{WT}}}{k_{\text{WT}}} \right)$$

with $V_{0.5}$ representing the voltage of half activation and k the slope of the curve at $V_{0.5}$ (see Table 1). The shifts of the steady-state activation curves (ΔV_{act}) of the Ca_v1.2 mutants

Table 1 Pore mutations affect voltage-dependent gating of $\text{Ca}_v1.2$

Mutant	V_{act} , mV	k , mV ^a	ΔG , kcal/Mol	I_{max} , pA/pF
Wild-type	-18.6±0.9 (8)	5.9±0.6		15.1±2.8
IS6 segment				
L434A	-39.3±0.9 (5)	5.9±0.8	-2.03±0.57	13.3±2.5
L434G	-32.3±0.7 (7)	7.6±0.7	-0.63±0.31	15.7±2.8
L434N	-22.0±0.8 (6)	6.5±0.7	-0.11±0.30	12.3±2.1
L434T	-30.8±1.3 (6)	6.9±0.9	-0.76±0.41	17.1±3.0
L434V	-32.6±0.8 (5)	5.9±0.7	-1.37±0.44	12.6±2.7
L434M	-23.0±1.2 (6)	4.6±0.7	-1.08±0.51	14.3±3.2
L434S	-28.9±0.7 (6)	5.0±0.5	-1.55±0.42	13.7±2.2
L434W	No current			
L434P ^b	No current			
IIIS6 segment				
F1191T	-25.7±1.0 (6)	7.1±0.8	-0.26±0.32	9.6±2.5
V1192T	-16.4±0.9 (7)	6.9±0.9	0.45±0.28	9.1±2.2
G1193T	-49.8±1.0 (7)	5.1±0.6	-3.89±0.72	17.5±3.2
G1193V	-38.1±0.7 (8)	5.6±0.6	-2.14±0.48	12.3±2.7
G1193N	-46.5±1.0 (5)	5.6±0.8	-2.99±0.73	11.2±2.9
G1193M	-33.6±0.7 (8)	6.4±0.6	-1.22±0.36	8.4±2.0
G1193A	-12.1±1.0 (6)	5.7±0.7	0.60±0.28	9.3±1.8
G1193Q	-39.2±0.8 (5)	7.0±0.7	-1.42±0.39	9.8±2.1
G1193P	-37.7±0.7 (7)	6.3±0.6	-1.63±0.39	11.3±2.7
G1193W	No current			
F1194T	-16.5±0.9 (7)	7.8±0.9	0.61±0.26	17.3±3.2
V1195T	-28.9±0.7 (7)	5.1±0.7	-1.48±0.51	18.7±3.4
I1196T	-26.6±0.6 (9)	4.9±0.6	-1.31±0.44	18.4±2.7

Midpoints and slope factors of the activation curves, maximal peak current densities and free energies of channel opening (ΔG) of the mutant channels are indicated. Numbers of experiments are indicated in parentheses

^a Changes of slope factors of mutated channels are statistically not significant ($p > 0.05$) compared to WT

^b Data from Kudrncak et al. [22]

compared to wild-type channels and the calculated changes in free energy ΔG were plotted against the descriptor values and analysed as described above for ΔV_{act} (see Supplemental data).

Results

G1193 is a gating-sensitive residue in IIIS6

We have recently shown that gradual changes in hydrophobicity in the bundle-crossing region of transmembrane segment IIS6 gradually shift the activation curve of $\text{Ca}_v1.2$ [17]. To investigate whether hydrophobic interactions play a similar role in the equivalent section of segment IIIS6, we substituted the small and polar threonine for each of several hydrophobic residues (F1191–I1196) of the $\text{Ca}_v1.2$ α_1 -subunit (Fig. 1a). Barium (Ba^{2+}) currents were subsequently measured with the patch-clamp technique after co-expression of the auxiliary β_{2a} and $\alpha_2\text{-}\delta_1$ subunits in tsA-201 cells. All six threonine mutants (F1191T–I1196T) conducted ionic currents. The largest shift in channel activation ($\Delta V_{\text{act}} = -31.2 \pm 1.3$ mV)

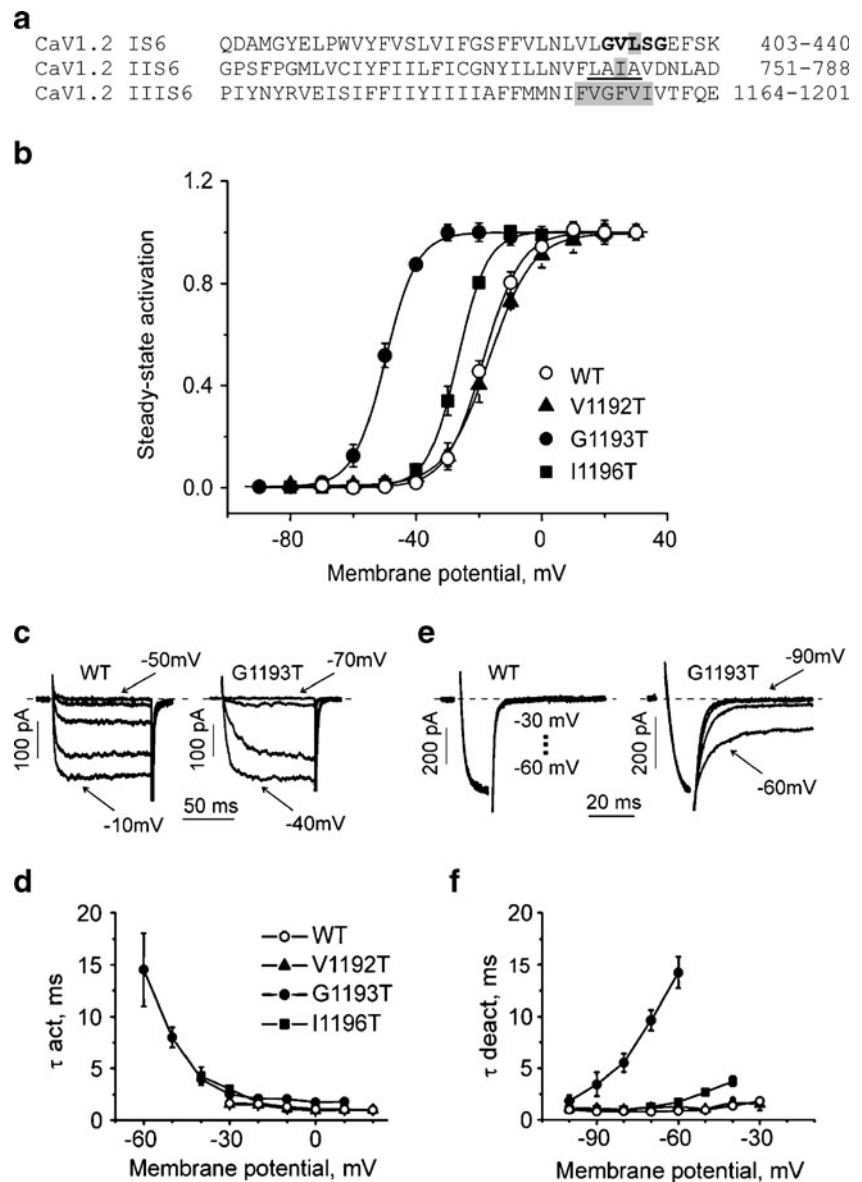
and the correspondingly slowest kinetics of current activation and deactivation were observed for mutation G1193T, suggesting a potentially important role of this glycine in $\text{Ca}_v1.2$ gating (Table 1; G1193 is ten residues downstream from the putative glycine hinge position). A family of inward Ba^{2+} currents and the corresponding activation curve of mutant G1193T are shown in Fig. 1. The activation time constant of G1193T ranged between 14.5 ms (-60 mV) and 1.8 ms (10 mV; Fig. 1d) and the deactivation time constant between 1.8 ms (-100 mV) and 14.2 ms (-60 mV).

Smaller kinetic changes were observed for mutations V1195T ($\Delta V_{\text{act}} = -10.3 \pm 1.1$ mV), I1196T ($\Delta V_{\text{act}} = -8.0 \pm 1.1$ mV) and F1191T ($\Delta V_{\text{act}} = -7.1 \pm 1.3$ mV). Other threonine substitutions had negligible effects (Table 1; see Fig. 1d, f for corresponding changes in current activation and deactivation kinetics of representative mutants V1192T, G1193T and I1196T compared to wild-type $\text{Ca}_v1.2$).

Mutating G1193 to residues with different properties

To gain insight into the structural requirements for stabilisation of the closed state of the channel at this position, we then replaced G1193 with a series of residues of different

Fig. 1 Gating changes induced by threonine mutations in segment IIIS6 of $Ca_v1.2$. **a** Alignment of pore-lining S6 segments of $Ca_v1.2$. Mutated residues are shaded grey. Previously identified gating determinants are *underlined*. GxxxG motif is shown in *bold*. **b** Averaged activation curves of wild-type ($n=8$) and mutants V1192T ($n=7$), G1193T ($n=7$) and I1196T ($n=9$). **c** Representative families of I_{Ba} through wild-type and G1193T mutant channels during depolarising test pulses from -100 mV. Zero current levels are indicated as dotted lines. **d** Mean time constants of channel activation of WT ($n=8$) and mutants V1192T ($n=7$), G1193T ($n=7$) and I1196T ($n=9$) are plotted against test potential. **e** Representative tail currents of WT and G1193T channels. Currents were activated during a 20-ms conditioning depolarisation to -10 mV for wild-type and -40 mV for G1193T. Deactivation was recorded during subsequent repolarisations with 10-mV increments starting from -100 mV. **f** Mean time constants of channel deactivation of wild-type ($n=7$) and mutants V1192T ($n=6$), G1193T ($n=6$) and I1196T ($n=7$) are plotted against test potential. Time constants were estimated by fitting current activation and deactivation to a mono-exponential function



hydrophobicity, size and polarity. The resulting changes in voltage dependence of $Ca_v1.2$ are illustrated in Fig. 2a. Replacement of G1193 by threonine, asparagine, glutamine, valine, methionine, proline and alanine shifts channel activation ranging from ΔV_{act} of -27.9 ± 1.3 mV for G1193N to 6.5 ± 1.3 mV for G1193A (Fig. 2a; Table 1). Interestingly, the mutation G1193A shifted the activation curve towards more depolarised voltages ($\Delta V_{act} = 6.5 \pm 1.3$ mV). Replacement of G1193 by tryptophan results in a non-functional channel. The larger shifts in channel activation in the hyperpolarising direction were accompanied by slower kinetics of current activation and deactivation (Fig. 2b, c). We observed no significant effects on the reversal potential (data not shown) suggesting that the studied deep pore mutations did not affect selectivity.

Mutation correlation analysis in position G1193

In order to get insights into possible links between channel activation and physicochemical properties of amino acids, regression analysis was performed for selected descriptors (see “Materials and methods” section and Supplementary Table 1), including size, hydrophobicity, flexibility and rigidity indices, propensity to van der Waals interactions and others.

Descriptor values were calculated with MOE or taken from the literature (see “Materials and methods”) and plotted against the corresponding shifts of the activation curves or calculated changes in free energy (ΔG). The correlations were ranked by correlation coefficient and significance. The best correlation with ΔV_{act} in position

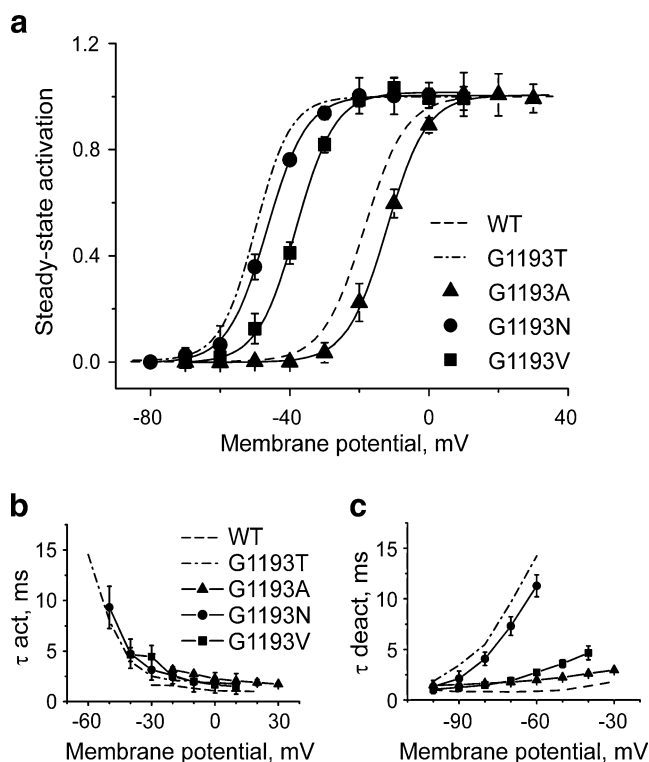


Fig. 2 Gating changes induced by mutations of G1193 in segment IIS6 of $\text{Ca}_v1.2$. **a** Averaged activation curves of the WT ($n=8$) and mutants G1193T ($n=7$), G1193A ($n=6$), G1193N ($n=5$) and G1193V ($n=8$). **b, c** Mean time constants of channel activation (**b**) and deactivation (**c**) for WT and mutants G1193T, G1193A, G1193N and G1193V are plotted against test potential ($n=5-8$). Time constants were estimated by fitting current activation and deactivation to a mono-exponential function

G1193, with the highest statistical significance (t test, $p < 0.009$), was obtained with the accessible surface area of all polar atoms (ASA_P; Fig. 3). Table 2 shows the correlation coefficients (r) for the linear regression plots of physicochemical descriptors against the measured ΔV_{act} . In contrast to our findings in segment IIS6 [17], ΔV_{act} did not correlate with hydrophobicity (Table 2). We subsequently searched for optimal two-descriptor correlations by combining all 17 descriptors in pairs (see “Materials and methods”). The most significant correlation was observed for the combination of ASA_P (leading descriptor) and the number of rotatable bonds (Fig. 3). Potentially modulating effects of other physicochemical properties are summarised in Table 3.

Correlation analysis in gating-sensitive position L434 (IS6)

A similar methodological approach was used to estimate the predictive value of amino acid properties for mutations in position L434. This amino acid was previously identified as a gating-sensitive residue in segment IS6 [22]. Mutating L434 to eight amino acids with different properties

(compare with mutations in segment IIS6) resulted in different shifts of the activation curve (Fig. 4).

The best prediction of ΔV_{act} was observed for the number of rotatable bonds (b_RotN, see Table 2). A rotatable bond is defined as any single non-ring bond to a non-terminal heavy atom within the amino acid molecule. The regression line for b_RotN is illustrated in Fig. 5 ($r=0.86$, $p < 0.006$). No improvement was observed for any combined descriptor correlation (Table 3).

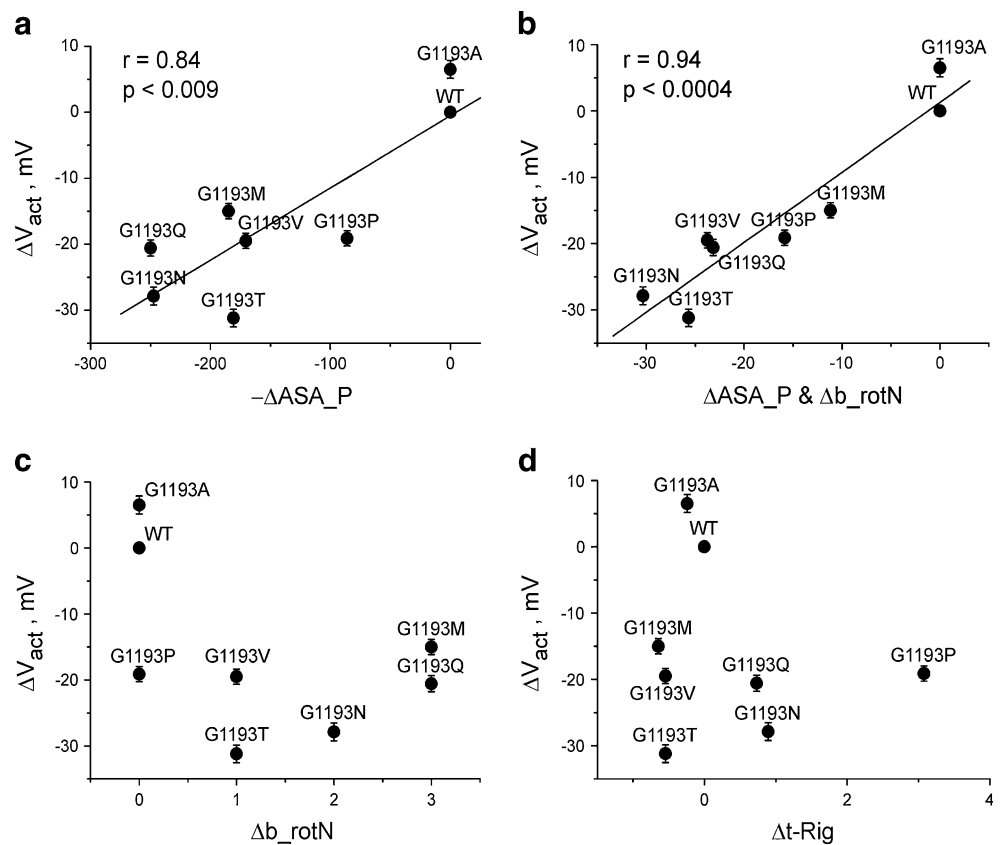
Modulation of hydrophobic interactions in I781 (IIS6) by other amino acid properties

In a previous study, we found a highly significant correlation between changes in hydrophobicity (ΔH) and ΔV_{act} for mutations in position I781 of segment IIS6 [17]. This correlation suggested that either the closed channel state is stabilised by hydrophobic interactions with neighbouring residue or a stabilisation of the open state by exposure of more polar residues in this position to water, or both. Here we confirmed the leading role of hydrophobicity in this position by accounting for all 17 descriptors in this position ($r=0.86$ and $p < 0.005$; see Table 3). Improved correlations were obtained for several descriptor combinations (e.g. hydrophobicity and the number of O and N atoms, with $r=0.97$ and $p < 0.0001$; see Table 3 for improved correlations for other amino acid properties).

Discussion

We have previously reported that the shift of the activation curve induced by point mutations in segment IIS6 correlates with changes in hydrophobicity in a cluster of residues in segment IIS6 (779–784: LAIA) and particularly in position I781 (see [17] for review). Mutations of I781 in the $\alpha 1$ subunit of $\text{Ca}_v1.2$ to residues of different hydrophobicity, size and polarity all shifted channel activation in the hyperpolarising direction with I781P causing the most severe (-37 mV shift) effect [19]. Mutations in position I781 decelerated activation and deactivation, and the shifts to more hyperpolarized voltages usually correlate with slower activation kinetics. Similar shifts of the activation curve and even more dramatic slowing of the activation and deactivation kinetics were observed in NaChBac when a conserved glycine 219 (corresponding to a putative hinge glycine in S6 of most K^+ channels) was mutated to a helix breaking proline [35]. Furthermore, when a locus of conserved hydrophobic residues in pore/gate-forming segment IVS6 of $\text{Ca}_v2.3$ (1718–1722: VAVIM) was systematically replaced by flexible glycines, slow deactivation of mutants A1719G and V1720G was accompanied by a -20 -

Fig. 3 The accessible surface area of all polar atoms in position G1193 (IIS6) predicts the shift of the activation curve. **a** Correlation between the shifts of the activation curves (ΔV_{act}) and the changes in accessible surface area of all polar atoms (ΔASA_P). **b** Correlation between ΔV_{act} and the best linear combination of two descriptors ASA_P and b_{rotN} (the number of rotatable bonds, see Table 3 for ranking). **c, d** No correlation between ΔV_{act} and Δb_{rotN} and ΔV_{act} and $\Delta t-Rig$ (an amino acid side-chain rigidity index). See complete list of descriptors in Supplementary Table 1



mV shift of the activation curve [27]. Thus, leftward shifts of the activation curve and slowing down of current activation in Ca_V are induced by mutations to amino acids with different physicochemical properties. Interestingly, the leftward shifts in the steady-state activation curves and the deceleration of the activation and deactivation resemble very much the action of L-type Ca^{2+} channel agonists such as BayK 8644 (see also [19]). Here we investigate whether these properties (descriptors) predict the measured shifts of the activation curve.

G1193 is a gating-related residue in segment IIS6

Mutating the hydrophobic residues of the ‘bundle-crossing’ region of segment IIS6 (Fig. 1a) to the small and polar threonine revealed a gating-sensitive residue at position G1193. Mutations of G1193 caused the largest changes in gating of $Ca_V1.2$ as measured by activation curves and current deactivation kinetics (Figs. 1b–f and 2).

Changes in the accessible surface area of all polar atoms in position G1193 (IIS6) predict the shifts of the activation curve

Crystal structures of KcsA, KvAP and MthK potassium channels revealed that a flexible glycine at analogous

positions 99, 220 and 83 provides a hinge point for helix bending of Kv during channel opening [21, 24, 35]. Mutation of the analogous glycine in NaChBac (G219P) to proline, which forces an α -helix into a bent conformation, substantially slowed deactivation and shifted the activation curve [36]. The functional role of S6 glycines and the positions for helix bending during channel activation of Ca_V remain unclear. No correlations either with side-chain rigidity or with helix turn propensity were observed for mutations of G1193 (Fig. 3d; Table 2; localised ten residues downstream from the putative glycine hinge position). We then examined the effect of side-chain size because we suspected that if the structure around G1193 were tightly packed, the small size of glycine might be functionally important. No significant correlation with the mass of the substituted residues was found ($p > 0.05$; Table 3). However, a significant correlation between ΔV_{act} and the accessible surface area of all polar atoms was observed (ASA_P ; Fig. 3a, b). Since ASA_P would indicate more favourable energy for solvation in water [8, 29, 31] than packing in the interior of a protein, this relationship suggests that the open gate conformation either exposes this position to more water than the closed conformation or allows the side chain to avoid unfavourable interactions with other residues, or both.

Table 2 Identification of leading descriptors predicting ΔV_{act}

Descriptor	<i>r</i>	<i>p</i>
L434 substitutions in segments IS6		
b_rotN	0.8695	0.0050
t-Flx	0.8690	0.0050
b_rotR	0.8551	0.0068
a_heavy	0.7793	0.0226
Weight	0.7761	0.0235
ASA	0.7685	0.0258
vdw_area	0.7533	0.0309
vdw_vol	0.7273	0.0408
...		
I781 substitutions in segments IIS6		
Hydrophobicity ^a	0.8679 ^c	0.0042
t-Rig	-0.6910	0.0577
vdw_area	0.6648	0.0720
a_count	0.6538	0.0786
b_rotR	0.6378	0.0888
vdw_vol	0.6149	0.1047
...		
G1193 substitutions in segments IIIS6		
ASA_P	-0.8438	0.0084
a_heavy	-0.7567	0.0297
b_count	-0.6928	0.0567
a_count	-0.6890	0.0587
Weight	-0.6862	0.0602
lip_don	-0.6834	0.0616
vdw_vol	-0.6609	0.0743
...		
Hydrophobicity	0.38397	0.34769
Helix turn propensity ^b	-0.1713	0.6849

The capability of a given descriptor to predict the shift of the activation curve was established by ranking the correlation coefficients (*r*) and its significance (*t* test). This approach enabled the identification of a 'leading descriptor' (L434—b_rotN; I781—hydrophobicity; G1193—ASA_P, see "Materials and methods")

^aHydrophobicity scale from Kyte and Doolittle [23]. Similar correlations were obtained with other scales [9, 13, 18, 20, 32]

^bMonné et al. [25]

^cData from Hering et al. [17]

Number of rotatable bonds and a side-chain amino acid flexibility index predict the shift of the activation curve by mutations in position L434 (IS6)

A strong correlation ($r=0.86$, $p<0.006$) between the number of rotatable bonds and ΔV_{act} was observed for mutations of L434 in segment IS6 (Figs. 4 and 5). These data suggest that a certain degree of side-chain flexibility of residues in this position of the 'bundle-crossing region' is

necessary for normal channel gating. A flexibility index introduced by Gottfries and Eriksson [11] for amino acids confirms the role of side-chain flexibility in this position. Interestingly, the gating-sensitive L434 occupies the central position of a GxxxG motif (Fig. 1a) which is known to allow backbone–backbone helix interactions in a hydrophobic environment [5]. The GxxxG motif participates in helix packing typically in a way where glycines allow close contacts between helices crossing at angles atypical of 'knobs-into-holes' packing. Other larger residues in these positions would probably tend to clash with atoms of the adjacent helix. L434 is located in the middle of this pattern (i.e. on the opposite face) and thus would not be involved in the helix–helix interactions that involve the glycines. We speculate that L434 is involved in interactions with other helices (e.g. if the glycines are involved with S6–S6 interactions than L434 could interact with S5 or L45 linker).

Co-correlations provide additional insight into modulatory properties of amino acid residues

In positions L434 (IS6), I781 (IIS6) and G1193 (IIIS6), we identified different leading descriptors providing the highest correlations with a single amino acid descriptor. A side-chain flexibility index, hydrophobicity and the accessible surface area of polar atoms predicted the shifts of the

Table 3 Combined descriptor analysis

Best linear combination of descriptors	<i>R</i>	<i>p</i>
L434 substitutions in segments IS6		
None of the 136 tested linear combinations improved the prediction of the leading descriptor	–	–
I781 substitutions in segments IIS6		
Hydrophobicity (68%)+lip_acc (32%)	0.9733	<0.0001
Hydrophobicity (68%)+b_rotN (32%)	0.9567	0.0001
Hydrophobicity (68%)+t-Flx (32%)	0.9477	0.0003
Hydrophobicity (73%)+ASA_P (27%)	0.9343	0.0006
Hydrophobicity (63%)+vdw_area (37%)	0.9266	0.0009
G1193 substitutions in segments IIIS6		
–ASA_P (67%)+b_rotN (33%)	0.9455	0.0003
–ASA_P (67%)+t-Flx (33%)	0.9232	0.0010

Correlations of weighted linear combinations of all 17 descriptors (see Supplementary Table 1) with ΔV_{act} . Combined descriptors were calculated as $\Delta D = a\Delta D_1 + b\Delta D_2$ (see "Materials and methods"). Weighting factors (*a* and *b*) were used to estimate the contribution of each descriptor to correlation. The fractional impacts of two amino acid descriptors in regression are indicated in percent. The capability of a given descriptor combination to predict the shift of the activation curve was established by ranking the correlation coefficients (*r*) and its significance (*t* test)

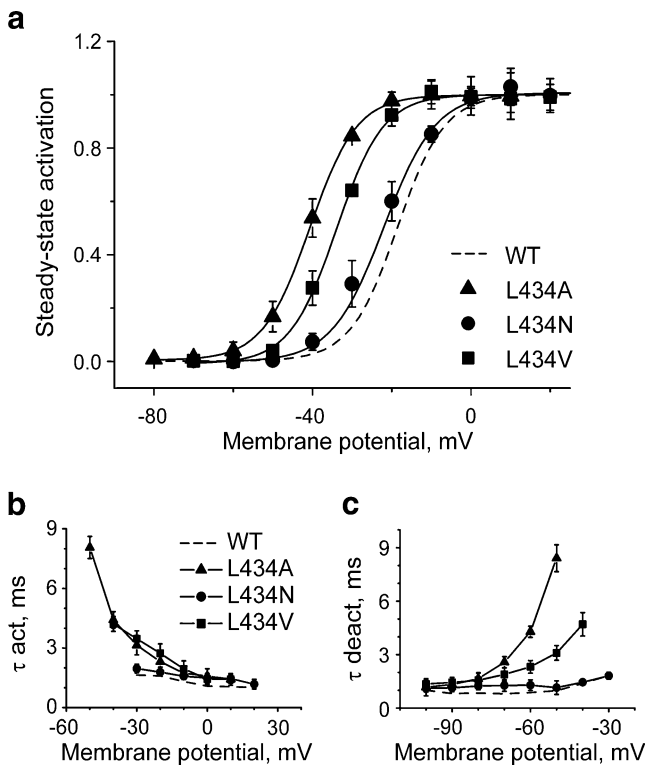
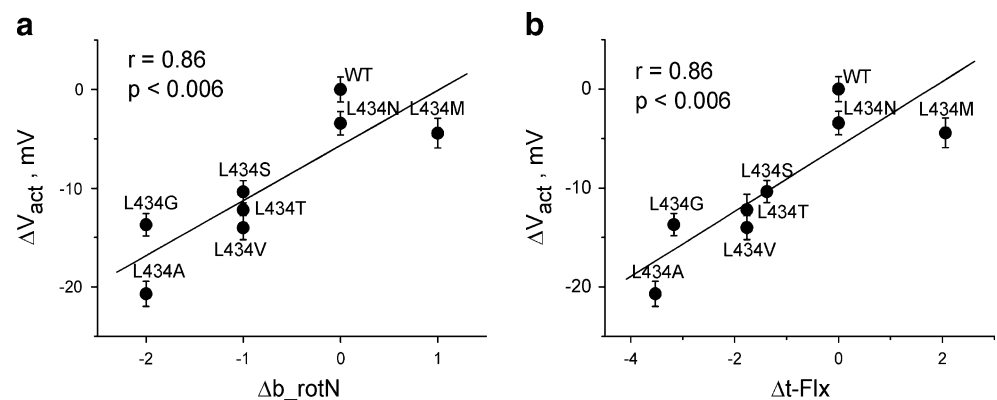


Fig. 4 Gating changes induced by mutations of L434 in segment IS6 of $Ca_v1.2$. **a** Averaged activation curves of the WT ($n=8$) and mutants L434A ($n=5$), L434N ($n=6$) and L434V ($n=5$). **b**, **c** Mean time constants of channel activation (**b**) and deactivation (**c**) for WT and mutants L434A, L434N and L434V are plotted against test potential ($n=5-8$). Time constants were estimated by fitting current activation and deactivation to a mono-exponential function

activation curves induced by mutations in the corresponding positions (Figs. 3, 5 and 6). We performed a co-correlation analysis where ΔV_{act} was correlated with any of the 136 weighted linear combination of two descriptors (see Supplementary Table 1 for complete list of descriptors combined for co-correlations). The predictive capability of side-chain flexibility in position L434 (i.e. number of rotatable bonds or the related amino acid descriptor

Fig. 5 Side-chain flexibility in position L434 (IS6) predicts the shifts of the activation curve. **a** Correlation between ΔV_{act} and Δb_{rotN} (number of rotatable bonds). **b** Correlation with the amino acid flexibility index $\Delta t\text{-Flx}$ (see Supplementary Table 1)



$\Delta t\text{-Flx}$) was not improved by any of the 136 co-correlations tested.

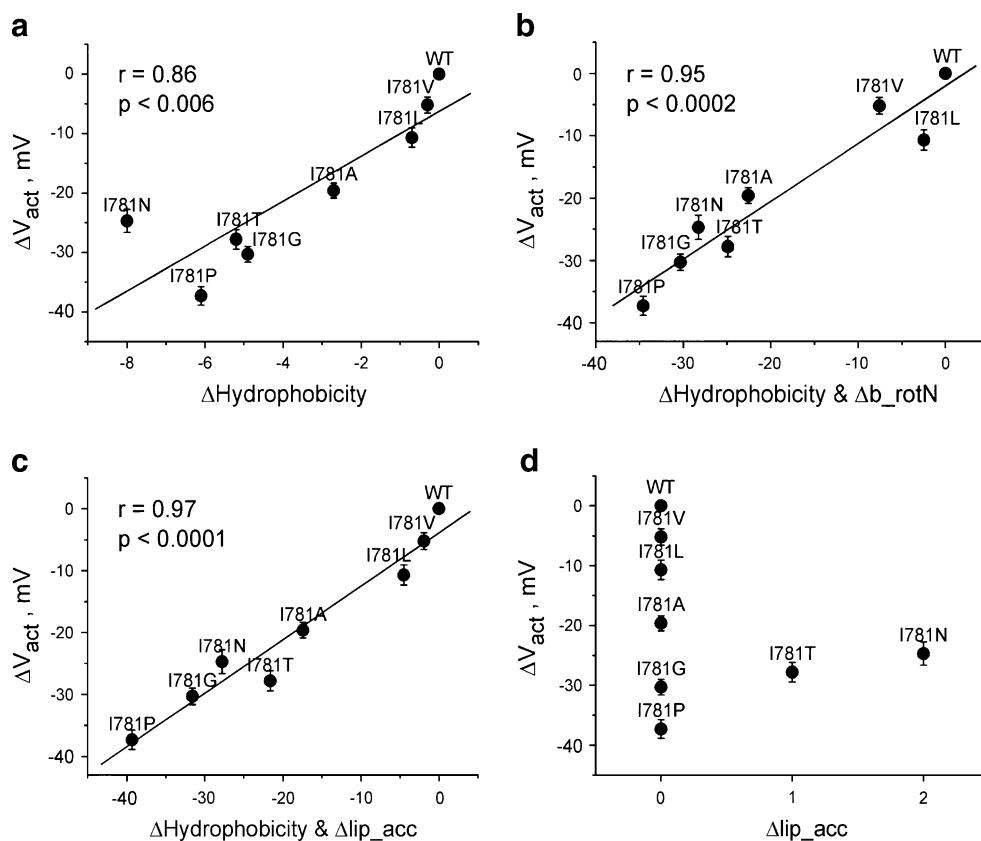
Analysing all linear combinations between two descriptors for mutations in position I781 and G1193 revealed some very strongly linear predictions of ΔV_{act} . The leading descriptor was found to be always one out of the best correlating descriptor pairs. The fractional weighting of the leading descriptors in the best-ranking combinations ranged from 60% to 83% (see Table 3, examples are illustrated in Figs. 3b and 6b, d). The second descriptors alone had no predictive capability (Figs. 3c and 6d). The best prediction of ΔV_{act} for mutations in position I781 was obtained for a combination of Δ Hydrophobicity and the number of hydrogen bond acceptors (N and O atoms) with second best ranking of the combination Δ Hydrophobicity and a side-chain flexibility index. These data suggest that hydrogen bonding and side-chain flexibility in this position affect the closed-open equilibrium. The same analysis for mutations in position G1193 revealed better correlations for the combination of the accessible surface area of all polar atoms with one of the side-chain flexibility.

The improved predictive capability of combined descriptors suggests that the dominating interaction (leading descriptor) in selected positions can be modulated by additional interactions (see Table 3 for other potentially modulating interactions in position I781, e.g. side-chain flexibility, van der Waals interactions and others).

Link between ΔV_{act} and changes in free energy (ΔG)

Replacing pore residues by amino acids with different physicochemical properties affects the free energy of $Ca_v1.2$ gating. Estimation of changes in free energies and cycle mutant analyses in voltage-gated ion channels enabled important insights into the energetics of channel opening (e.g. [30, 33]; see [22] for a study on $Ca_v1.2$). Accordingly, we have calculated the changes of free energy during the activation of wild-type and all IS6,

Fig. 6 Hydrophobicity in position I781 (IIS6) predicts the shifts of the activation curve. **a** Correlation between ΔV_{act} and changes in hydrophobicity. **b** The best prediction of ΔV_{act} by a linear combination of two descriptors was obtained for $\Delta\text{Hydrophobicity}$ and $\Delta\text{lip_acc}$ (number of O and N atoms; hydrogen bond acceptors). **c** Second best co-correlation was observed for $\Delta\text{Hydrophobicity}$ and $\Delta\text{b_rotN}$ (see also Table 3). **d** No correlation between ΔV_{act} and $\Delta\text{lip_acc}$ (see Supplementary Table 1)



IIS6 and IIS6 $\text{Ca}_v1.2$ mutants. ΔV_{act} and ΔG correlate strongly (Supplementary Figure 1). Nevertheless, ΔG deduced from a Boltzmann distribution reflects not only the energy of pore opening but also the energy of voltage sensor transition. In general, it can be assumed that mutations in the pore region do not disturb the voltage sensor transition and that ΔG of S6 mutations reflects the changes in the pore. However, some mutations apparently affect the transition of the voltage-sensing machinery from the resting to the activated state (e.g. I780P (IIS6) in [2]). Changes in the slope factor reflect changes in $\delta \times Z$, where Z is the charge and δ is a fraction of membrane potential that the voltage sensors cross during their movement. Obviously the mutations in the pore are unable to change the charge Z . They may, however, modify the fraction of the effective membrane potential by releasing or restricting voltage sensor movements. Minor changes in the slope factor (see Table 1) have effects on the calculated ΔG and may affect correlations. For the studied S6 mutations, ΔG and ΔV_{act} appeared to be equivalent measures of the pore energetics. This may, however, not always be the case and care has to be taken with pore mutations that significantly change the slope factor (e.g. I1196T; Table 1) or significantly change the kinetics of channel opening and closure (A780P [2]).

Conclusions and outlook

Mutations in the bundle-crossing region of pore-forming S6 segments frequently shift the activation curves along the voltage axis and affect the kinetics of channel gating. Making use of mutation correlation analysis, we identified descriptors of side chains at specific positions that predict these changes in channel activation gating. In segment IS6 (L434), ΔV_{act} correlated with the number of rotatable bonds reflecting side-chain flexibility. In position G1193 in segment IIS6, ΔV_{act} depended on the accessible surface area of all polar atoms, and in position I781, ΔV_{act} correlated with hydrophobicity. Leading descriptors were identified by single and combined correlation analysis (i.e. correlations between ΔV_{act} and all possible pairs of amino acid descriptors were analysed). Correlation analysis emerges thus as a useful tool to unravel the importance of particular amino acid properties in pore-lining S6 segments. Different leading descriptors in different S6 segments indicate individual contributions of four homologous but not identical domains in $\text{Ca}_v1.2$ gating.

Acknowledgement We would like to thank Bob Guy for very valuable comments on the manuscript and Gerhard Ecker for helpful

suggestions. Research was supported by FWF grants P19614 (SH) and P22600 (SB).

Open Access This article is distributed under the terms of the Creative Commons Attribution Noncommercial License which permits any noncommercial use, distribution, and reproduction in any medium, provided the original author(s) and source are credited.

References

- Berridge MJ (2003) Cardiac calcium signalling. *Biochem Soc Trans* 31:930–933
- Beyl S, Kügler P, Kudrncac M, Hohaus A, Hering S, Timin E (2009) Different pathways for activation and deactivation in CaV1.2: a minimal gating model. *J Gen Physiol* 134:231–241
- Beyl S, Timin EN, Hohaus A, Sary A, Kudrncac M, Guy RH, Hering S (2007) Probing the architecture of an L-type calcium channel with a charged phenylalkylamine: evidence for a widely open pore and drug trapping. *J Biol Chem* 282:3864–3870
- Blaber M, Zhang XJ, Matthews BW (1993) Structural basis of amino acid alpha helix propensity. *Science* 260:1637–1640
- Brosig B, Langosch D (1998) The dimerization motif of the glycoporphin A transmembrane segment in membranes: importance of glycine residues. *Protein Sci* 7:1052–1056
- Catterall WA (2000) Structure and regulation of voltage-gated Ca²⁺ channels. *Annu Rev Cell Dev Biol* 16:521–555
- Catterall WA, Perez-Reyes E, Snutch TP, Striessnig J (2005) International Union of Pharmacology. XLVIII. Nomenclature and structure–function relationships of voltage-gated calcium channels. *Pharmacol Rev* 57:411–425
- Chothia C (1974) Hydrophobic bonding and accessible surface area in proteins. *Nature* 248:338–339
- Eisenberg D, Weiss RM, Terwilliger TC (1984) The hydrophobic moment detects periodicity in protein hydrophobicity. *Proc Natl Acad Sci U S A* 81:140–144
- Ellis SB, Williams ME, Ways NR, Brenner R, Sharp AH, Leung AT, Campbell KP, McKenna E, Koch WJ, Hui A et al (1988) Sequence and expression of mRNAs encoding the alpha 1 and alpha 2 subunits of a DHP-sensitive calcium channel. *Science* 241:1661–1664
- Gottfries J, Eriksson L (2009) Extensions to amino acid description. *Mol Divers*. doi:10.1007/s11030-009-9204-2
- Grabner M, Dirksen RT, Beam KG (1998) Tagging with green fluorescent protein reveals a distinct subcellular distribution of L-type and non-L-type Ca²⁺ channels expressed in dysgenic myotubes. *Proc Natl Acad Sci U S A* 95:1903–1908
- Guy HR (1985) Amino acid side-chain partition energies and distribution of residues in soluble proteins. *Biophys J* 47:61–70
- Hackos DH, Chang TH, Swartz KJ (2002) Scanning the intracellular S6 activation gate in the shaker K⁺ channel. *J Gen Physiol* 119:521–532
- Hamill OP, Marty A, Neher E, Sakmann B, Sigworth FJ (1981) Improved patch-clamp techniques for high-resolution current recording from cells and cell-free membrane patches. *Pflugers Arch* 391:85–100
- Hemara-Wahanui A, Berjukow S, Hope CI, Dearden PK, Wu SB, Wilson-Wheeler J, Sharp DM, Ludson-Treweek P, Clover GM, Hoda JC, Striessnig J, Marksteiner R, Hering S, Maw MA (2005) A CACNA1F mutation identified in an X-linked retinal disorder shifts the voltage dependence of Cav1.4 channel activation. *Proc Natl Acad Sci U S A* 102(21):7553–7558
- Hering S, Beyl S, Sary A, Kudrncac M, Hohaus A, Guy HR, Timin E (2008) Pore stability and gating in voltage-activated calcium channels. *Channels* 2:61–69
- Hessa T, Kim H, Bihlmaier K, Lundin C, Boekel J, Ersson H, Nilsson I, White SH, von Heijne G (2005) Recognition of transmembrane helices by the endoplasmic reticulum translocon. *Nature* 433:377–381
- Hohaus A, Beyl S, Kudrncac M, Berjukow S, Timin EN, Marksteiner R, Maw MA, Hering S (2005) Structural determinants of L-type channel activation in segment IIS6 revealed by a retinal disorder. *J Biol Chem* 280:38471–38477
- Hopp TP, Woods KR (1981) Prediction of protein antigenic determinants from amino acid sequences. *Proc Natl Acad Sci U S A* 78:3824–3828
- Jiang Y, Lee A, Chen J, Cadene M, Chait BT, MacKinnon R (2002) The open pore conformation of potassium channels. *Nature* 417:523–526
- Kudrncac M, Beyl S, Hohaus A, Sary A, Peterbauer T, Timin E, Hering S (2009) Coupled and independent contributions of residues in IS6 and IIS6 to activation gating of CaV1.2. *J Biol Chem* 284:12276–12284
- Kyte J, Doolittle RF (1982) A simple method for displaying the hydropathic character of a protein. *J Mol Biol* 157:105–132
- Magidovich E, Yifrach O (2004) Conserved gating hinge in ligand- and voltage-dependent K⁺ channels. *Biochemistry* 43:13242–13247
- Monné M, Nilsson I, Elofsson A, von Heijne G (1999) Turns in transmembrane helices: determination of the minimal length of a “helical hairpin” and derivation of a fine-grained turn propensity scale. *J Mol Biol* 293:807–814
- Perez-Reyes E, Castellano A, Kim HS, Bertrand P, Bagstrom E, Lacerda AE, Wei XY, Birnbaumer L (1992) Cloning and expression of a cardiac/brain beta subunit of the L-type calcium channel. *J Biol Chem* 267:1792–1797
- Raybaud A, Baspinar EE, Dionne F, Dodier Y, Sauvé R, Parent L (2007) The role of distal S6 hydrophobic residues in the voltage-dependent gating of CaV2.3 channels. *J Biol Chem* 282:27944–27952
- Raybaud A, Dodier Y, Bissonnette P, Simoes M, Bichet DG, Sauvé R, Parent L (2006) The role of the GX9GX3G motif in the gating of high voltage-activated Ca²⁺ channels. *J Biol Chem* 281(51):39424–39436
- Rose GD, Geselowitz AR, Lesser GJ, Lee RH, Zehfus MH (1985) Hydrophobicity of amino acid residues in globular proteins. *Science* 229:834–838
- Sadovsky E, Yifrach O (2007) Principles underlying energetic coupling along an allosteric communication trajectory of a voltage-activated K⁺ channel. *Proc Natl Acad Sci U S A* 104:19813–19818
- Sharp KA, Nicholls A, Friedman R, Honig B (1991) Extracting hydrophobic free energies from experimental data: relationship to protein folding and theoretical models. *Biochemistry* 30:9686–9697
- White SH, Wimley WC (1999) Membrane protein folding and stability: physical principles. *Annu Rev Biophys Biomol Struct* 28:319–365
- Yifrach O, MacKinnon R (2002) Energetics of pore opening in a voltage-gated K(+) channel. *Cell* 111:231–239
- Zhao Y, Scheuer T, Catterall WA (2004) Reversed voltage-dependent gating of a bacterial sodium channel with proline substitutions in the S6 transmembrane segment. *Proc Natl Acad Sci U S A* 101:17873–17878
- Zhao Y, Yarov-Yarovoy V, Scheuer T, Catterall WA (2004) A gating hinge in Na⁺ channels; a molecular switch for electrical signaling. *Neuron* 41:859–865
- Zhen XG, Xie C, Fitzmaurice A, Schoonover CE, Orenstein ET, Yang J (2005) Functional architecture of the inner pore of a voltage-gated Ca²⁺ channel. *J Gen Physiol* 126:193–204